



1 Characterization of nighttime formation of particulate organic 2 nitrates based on high-resolution aerosol mass spectrometry in an 3 urban atmosphere in China

4 Kuangyou Yu^{1,2,*}, Qiao Zhu^{1,*}, Ke Du², Xiao-Feng Huang¹

5 ¹Key Laboratory for Urban Habitat Environmental Science and Technology, School of Environment and Energy, Peking
6 University Shenzhen Graduate School, Shenzhen, 518055, China.

7 ²Department of Mechanical and Manufacturing Engineering, University of Calgary, Calgary, Canada.

8 * Authors have equal contribution.

9
10 **Abstract.** Organic nitrates are important atmospheric species that significantly affect the cycling of NO_x and ozone production.
11 However, characterization of particulate organic nitrates and their sources in inorganic nitrate-abundant particles in polluted
12 atmosphere is a big challenge, and has been little performed in the literature. In this study, an Aerodyne high-resolution time-
13 of-flight aerosol mass spectrometer (HR-ToF-AMS) was deployed at an urban site in South China from 2015 to 2016 to
14 characterize particulate organic nitrates with high time resolution. Based on two different data processing methods, 13-21% of
15 the total measured nitrates was identified to be organic nitrates in spring, 41-64% in summer and 16%-25% in autumn; however,
16 in winter, most measured nitrates were inorganic. The good correlation between organic nitrates and fresh secondary organic
17 aerosol identified by the positive matrix factorization method at night rather than in the daytime indicated a potentially
18 important role of nighttime secondary formation. Therefore, we theoretically estimated nighttime NO₃ radical concentrations
19 and SOA formation using the various VOCs measured simultaneously. Consequently, the calculated products of monoterpene
20 reacting with NO₃ agreed well with the organic nitrates in terms of both concentration and variation, suggesting that the
21 biogenic VOC reactions with NO₃ at night are the dominant formation pathway for particulate organic nitrates in polluted
22 atmosphere, despite of much higher abundance of anthropogenic VOCs.

24 1. Introduction

25 Organic nitrates in aerosols have an important impact on the fate of NO_x and ozone production (Lelieveld et al., 2016), which
26 can be formed in a minor channel of the reaction between peroxy radicals and NO (R1 and R2) (usually, an increased fraction
27 of this reaction leads to the formation of alkoxy radicals and NO₂ (R3)) or via the NO₃-induced oxidation of unsaturated
28 hydrocarbons (R4). Even though some recent studies have suggested that the formation of organic nitrates from

29
30 Correspondence to: X.-F. Huang (huangxf@pku.edu.cn)



31 peroxy radicals and NO may play a larger role than previously recognize unsaturated hydrocarbons (R4). Even though some
32 recent studies have suggested that the formation of organic nitrates from peroxy radicals and NO may play a larger role than
33 previously recognized, yields of organic nitrates via NO₃ reacting with alkenes are generally much higher (Teng et al., 2017,
34 2015).



39 Several direct methods have been developed to measure total organic nitrates (gas + particle) in the real atmosphere. For
40 example, Rollins et al.(2012) used a thermal-dissociation laser-induced fluorescence technique (TD-LIF) to observe total
41 organic nitrates in the United States; Sobanski et al. (2017) obtained organic nitrates in Germany using the thermal dissociation
42 cavity ring-down spectroscopy (TD-CRDS). However, it is still difficult to identify and quantify the particle phase organic
43 nitrates, which could contribute a large portion of secondary organic aerosol (SOA) (Rollins et al., 2012; Xu et al., 2015a; Fry
44 et al., 2013; Ayres et al., 2015; Boyd et al., 2015; Lee et al., 2016), using these direct measurement methods. Recently,
45 researchers have proposed some estimation methods for particle-phase organic nitrates based on aerosol mass spectrometry
46 (AMS) with high time resolution (Farmer et al., 2010; Hao et al., 2014; Xu et al., 2015a, 2015b). Ng et al. (2017) reviewed the
47 nitrate radical chemistry and the abundance of particulate organic nitrates at multiple sites of the world, but all of these sites
48 are located in the region (i.e. United States and Europe) with relatively clean air. To our best knowledge, few studies have
49 investigated the concentrations and formation pathways of particulate organic nitrates in the atmosphere with high
50 anthropogenic pollutants (Xu et al., 2017), especially with high particulate inorganic nitrate, which would make identification
51 of organic nitrates harder in aerosol mass spectrum.

52 South China is located in a subtropical region, where the photochemical reactions are extremely active (Zhang et al., 2008),
53 and the biogenic VOCs and anthropogenic NO_x are relatively high. To assess the evolution of particle-phase organic nitrates
54 in a more polluted atmosphere, in this study, we deployed Aerodyne high-resolution time-of-flight aerosol mass spectrometry
55 (HR-ToF-AMS) with other instruments over an urban site in South China from 2015 to 2016 to obtain submicron aerosols.
56 Then, organic nitrates and their contributions to OAs in different seasons were estimated by different methods based on the
57 HR-ToF-AMS measurements. Furthermore, we used the estimates combined with the measured VOC data to investigate the
58 potential pathway formation for organic nitrates in South China.



59 2. Experiment methods

60 2.1 Sampling site and period

61 The sampling site (22.6°N, 113.9°E; 20 m a.s.l) was on the roof of one academic building on the campus of the Peking
62 University Shenzhen Graduate School (PKUSZ), which is located in the western urban area in Shenzhen (Figure 1). This site
63 is mostly surrounded by subtropical plants without significant anthropogenic emission sources nearby, except for a local
64 road that is ~100 m from the site. In this study, we use the statistical data from the Meteorological Bureau of Shenzhen
65 Municipality (<http://www.szmb.gov.cn/site/szmb/Esztq/index.html>) as the reference data to determine the sampling periods
66 to obtain more representative samples in different seasons during 2015-2016, as shown in Table 1.



67
68 **Figure 1.** The location of the sampling site.

69 **Table 1.** Meteorological conditions, PM₁ species concentrations and relevant parameters in the estimation of organic nitrates
70 for different seasons in Shenzhen.

Sampling period		4.1-4.30, 2016	8.1-8.31, 2015	11.4-11.30, 2015	1.21-2.3, 2016
		Spring	Summer	Autumn	Winter
Meteorology	T (°C)	24.5±2.5	29.0±3.0	23.6±3.7	10.7±4.7
	RH (%)	78.0±12.7	71.2±17.5	68.2±15.8	75.4±18.7
	WS (m s ⁻¹)	1.4±0.8	1.0±0.7	1.2±0.7	1.5±0.8
Species	Org	4.3±3.2	10.0±6.9	7.8±5.9	5.1±3.5
	SO ₄ ²⁻	3.2±1.8	5.8±3.3	2.3±1.5	1.9±1.2
	NO ₃ ⁻	0.96±1.4	0.91±0.90	1.3±1.4	1.6±1.0



$(\mu\text{g m}^{-3})$	NH_4^+	1.4±0.8	2.0±1.1	1.1±0.8	1.2±0.6
	Cl^-	0.14±0.19	0.03±0.05	0.22±0.36	0.64±0.85
	BC	1.9±2.1	2.4±1.6	3.5±2.6	2.4±1.5
	PM_{10}	12.0±8.9	15.1±13.8	11.8±9.5	12.2±7.2
ON parameters	$R_{\text{NH}_4\text{NO}_3}$	2.80	3.20	3.32	3.48
	R_{obs}	3.74	6.14	4.30	3.55
	Fraction of positive data	99%	99%	84%	47%

71 2.2 Instrumentation

72 2.2.1 High Resolution Time-of-Flight Aerosol Mass Spectrometer

73 During the sampling periods, the chemical compositions and mass concentration of non-refractory PM_{10} were measured by an
 74 HR-ToF-AMS, and detailed descriptions of this instrument are given in the literatures (DeCarlo et al., 2006; Canagaratna et
 75 al., 2007). In summary, the HR-ToF-AMS focuses ambient particles with vacuum aerodynamic diameter smaller than $1 \mu\text{m}$
 76 into narrow beam via an aerodynamic lens, then the submicron particles are vaporized by impaction on a tungsten heated
 77 surface ($\sim 600 \text{ }^\circ\text{C}$) and ionized by electron ionization (70eV). Only non-refractory species can be vaporized and detected. The
 78 setup and operation of the HR-ToF-AMS can be found in our previous studies (Huang et al., 2010, 2012; Zhu et al., 2016). To
 79 remove coarse particles, a $\text{PM}_{2.5}$ cyclone inlet was placed on the roof of the building to introduce an air stream containing the
 80 remaining particles into a room through a copper tube with a flow rate of 10 l min^{-1} . Before entering the AMS, the samples
 81 are dried by a nafion dryer (MD-070-12S-4, Perma Pure Inc.) to eliminate the potential influence of relative humidity on the
 82 particle collection (Matthew et al., 2008). The ionization efficiency (IE) calibrations were performed by using pure ammonium
 83 nitrate particles on every two weeks. The relative IEs (RIEs) for organics, nitrate and chloride were assumed to be 1.4, 1.1 and
 84 1.3, respectively. A composition-dependent collection efficiency (CE) was applied to the data based on the method of
 85 Middlebrook et al. (2012). The instrument was operated at two ion optical modes with a cycle of 4 min, including 2 min for
 86 the mass-sensitive V-mode and 2 min for the high mass resolution W-mode. The HR-ToF-AMS data analysis was performed
 87 using the software SQUIRREL (version 1.57) and PIKA (version 1.16) written in Igor Pro 6.37 (Wave Metrics
 88 Inc.) (<http://cires1.colorado.edu/jimenezgroup/ToFAMSResources/ToFSoftware/index.html>).

89 2.2.2 Other co-located instruments

90 In addition to the HR-ToF-AMS, a suite of instruments was deployed in the same sampling site. An aethalometer (AE-31,
 91 Magee) was simultaneously used for measurements of refractory black carbon (BC) with a temporal resolution of 5 min. VOCs
 92 concentrations were measured via an automated in-situ gas chromatograph (Agilent 5977E) equipped with a mass spectrometer



93 (Agilent 5971). Ozone and NO_x was measured by a 49i ozone analyzer and a 42i nitrogen oxide analyzer (Thermo Scientific,
 94 US), respectively.

95 2.3 Organic nitrate estimation

96 In this study, we use two methods to estimate the organic nitrates based on AMS organic data, following the same analysis
 97 approach in Xu et al. (2015b). The first method for estimating organic nitrates is based on the NO⁺/NO₂⁺ ratio (NO_x⁺ ratio) in
 98 the HR-AMS spectrum. Due to their very different NO_x⁺ ratios (R_{ON} and $R_{NH_4NO_3}$) (Farmer et al., 2010; Boyd et al., 2015; Fry
 99 et al., 2008; Bruns et al., 2010), the NO₂ and NO concentrations for the organic nitrates ($NO_{2,ON}$ and NO_{ON}) can be quantified
 100 with the HR-AMS data via Eqs. (1) and (2), respectively (Farmer et al., 2010):

$$101 \quad NO_{2,ON} = \frac{NO_{2,obs} \times (R_{obs} - R_{NH_4NO_3})}{R_{ON} - R_{NH_4NO_3}} \quad (1)$$

$$102 \quad NO_{ON} = R_{ON} \times NO_{2,ON} \quad (2)$$

103 where R_{obs} is the NO_x⁺ ratio from the observation. The value of R_{ON} is difficult to determine because it varies between
 104 instruments and precursor volatile organic compounds (VOCs). However, $R_{ON}/R_{NH_4NO_3}$ has been assumed instrument-
 105 independent (Fry et al., 2013). In this study, we use $R_{ON}/R_{NH_4NO_3}$ estimation range (from 2.08 to 3.99) from the literature (Farmer
 106 et al., 2010; Boyd et al., 2015; Bruns et al., 2010; Sato et al., 2010) to determine R_{ON} due to the variation of precursor VOCs.
 107 It is important to note that if a large percentage of organic nitrates value are negative using this method, it is because the values
 108 of R_{obs} is smaller than $R_{NH_4NO_3}$, further indicating the inorganic nitrates contributes near all to the total nitrates.

109 The second method is based on the positive matrix factorization (PMF) analysis. In addition to the PMF of the organic mass
 110 spectra (Zhang et al., 2011; Ng et al., 2010; Huang et al., 2013), the same analysis of the HR organic mass spectra, combined
 111 with NO⁺ and NO₂⁺ ions was performed to identify the relative contributions of organic and inorganic nitrates (Hao et al.,
 112 2014; Xu et al., 2015b). In this study, the detailed PMF analysis procedure can be found in our previous publications (Huang
 113 et al., 2010; Zhu et al., 2016; He et al., 2011). For each season, three organic factors and one inorganic factor are identified: a
 114 hydrocarbon-like OA (HOA), a more-oxidized oxygenated OA (MO-OOA), a less-oxidized oxygenated OA (LO-OOA) and
 115 a nitrate inorganic aerosol (NIA). In this method, the NO⁺ and NO₂⁺ ions are distributed among different organic aerosol factors
 116 and NIAs; the concentration of the nitrate functionality in the organic nitrates ($NO_{3,org}$) is equal to the sum of NO⁺ and NO₂⁺
 117 in the organic nitrates (i.e., NO_{org}^+ and $NO_{2,org}^+$) via Eqs. (3) and (4), respectively (Xu et al., 2015b):

$$118 \quad NO_{org}^+ = \sum([OA \ factor]_i \times f_{NO_i}) \quad (3)$$

$$119 \quad NO_{2,org}^+ = \sum([OA \ factor]_i \times f_{NO_{2,i}}) \quad (4)$$

120 where $[OA \ factor]_i$ represents the mass concentration of the i th OA factor and f_{NO_i} and $f_{NO_{2,i}}$ represent the mass fractions of
 121 NO⁺ and NO₂⁺, respectively.

122 2.4 Nitrate radical estimation

123 In this section, the approach of nitrates radical estimation is similar to Xu et al. (2015a). The average concentration of VOCs
 124 and the reaction rate coefficients of NO₃ + VOCs at 25 °C are listed in Table S1. NO₃ is the product of NO₂+O₃, and its losses



125 react with individual VOCs, NO and photolysis. Due to the existence of N_2O_5 in equilibrium with $NO_2 + NO_3$, we should first
 126 estimate the sinks of N_2O_5 impacting the life of nitrate radicals. There are both heterogenous and homogeneous reactions of
 127 N_2O_5 with water. The N_2O_5 lifetime, with respect to the heterogeneous uptake of aqueous particles, is (Fry et al., 2013):

$$128 \quad \tau_{N_2O_5,het} = \frac{1}{K_{het}} = \frac{4SA}{\gamma v} \quad (5)$$

129 where K_{het} represents the rate of heterogeneous uptake, γ is the uptake coefficient, v represents the molecular speed, and SA
 130 represents the surface area of the particles. By using the upper-limit values of $\gamma = 0.04$ (Saunders et al., 2003), $v = 240 \mu m^2$
 131 $cm^{-3} s^{-1}$ and $SA = 220 \mu m^2 cm^{-3}$, we calculate $\tau_{N_2O_5,het}$ to be approximately 1760 s. In addition, the N_2O_5 lifetime, with
 132 respect to the reaction with H_2O , is (Crowley et al., 2011):

$$133 \quad \tau_{N_2O_5,H_2O} = \frac{1}{K_{H_2O}} = \frac{1}{2.5 \times 10^{-22} [H_2O] + 1.8 \times 10^{-39} [H_2O]^2} \quad (6)$$

134 K_{H_2O} represents the reaction rate of N_2O_5 and H_2O , and $[H_2O]$ represents the water concentration (unit of molecule cm^{-3}); the
 135 daily maximum $[H_2O]$ is 5.5×10^{11} molecule cm^{-3} at 6:00 during the sampling period, and the calculated value is 1.4×10^{10} s.

136 Then, we estimate the NO_3 lifetime by only considering the reaction with VOCs ($\tau_{NO_3,VOCs}$):

$$137 \quad \tau_{NO_3,VOCs} = \frac{1}{\sum k_i [VOC_i]} \quad (7)$$

138 The average lifetime of NO_3 is approximately 14.08 s. Based on the estimation of the N_2O_5 and NO_3 lifetimes above, we can
 139 conclude that the influence of N_2O_5 could be ignored when estimating the NO_3 concentration and, due to the high reactivity
 140 of NO_3 (14.08 s), the steady-state NO_3 can be predicted:

$$141 \quad [NO_3] = \frac{k_1 [O_3] [NO_2]}{J_{NO_3} + k_2 [NO] + \sum k_i [VOC_i]} \quad (8)$$

142 where J_{NO_3} is calculated from the solar zenith angles and NO_3 photolysis rates (Saunders et al., 2003) and, in this study, the
 143 typical value of J_{NO_3} is $0.12 s^{-1}$ during the daytime. k_1 is $3.52 \times 10^{-17} cm^3 molecule^{-1} s^{-1}$, and k_2 is $2.7 \times 10^{-11} cm^3 molecule^{-1} s^{-1}$
 144 according to the Master Chemical Mechanism model (<http://mcm.leeds.ac.uk/MCM/>; under 25 °C). The average
 145 concentrations of O_3 and NO_2 are 6.82 and 19.38 ppb, respectively.

146 3. Results and discussion

147 3.1 Results of the organic nitrate estimation

148 Table 2 shows the concentrations of nitrate functionality in organic nitrates (i.e., $NO_{3,org}$) and their contributions to the total
 149 measured nitrate, which is estimated by the NO^+/NO_2^+ ratio method and PMF method. Note that the small difference between
 150 the average R_{obs} and $R_{NH_4NO_3}$ in winter leads to a large portion of negative data (Table 1), which suggests that a very limited
 151 amount of organic nitrates contribute to the total nitrate, as discussed above; thus, we only discuss the organic nitrates in spring,
 152 summer and autumn. For the NO^+/NO_2^+ ratio method, two calculated R_{ON} values for each season based on the $R_{ON}/R_{NH_4NO_3}$
 153 estimation range (from 2.08 to 3.99) are applied to provide the upper and lower bounds of the estimated $NO_{3,org}$ mass



154 concentration. For the PMF method, the NO_x^+ ions were assigned to different PMF factors (Figure S1) due to the different
 155 physicochemical properties of the nitrate components. The NIAs are dominated by NO^+ and NO_2^+ but also contain some
 156 organic fragments, such as CO_2^+ and $\text{C}_2\text{H}_3\text{O}^+$, which agrees with the literature (Hao et al., 2014; Xu et al., 2015b; Sun et al.,
 157 2012). This indicates that the NIA factor experiences potential interference from organics. In addition, the $\text{NO}^+/\text{NO}_2^+$ ratio in
 158 NIAs is higher than that in pure NH_4NO_3 , which supports the underestimation of $\text{NO}_{3,\text{org}}$ concentrations with this method. This
 159 also explains why the concentration of $\text{NO}_{3,\text{org}}$ estimated using the PMF method is always close to the lower estimation of
 160 $\text{NO}_{3,\text{org}}$ via the $\text{NO}^+/\text{NO}_2^+$ ratio method in Table 2.

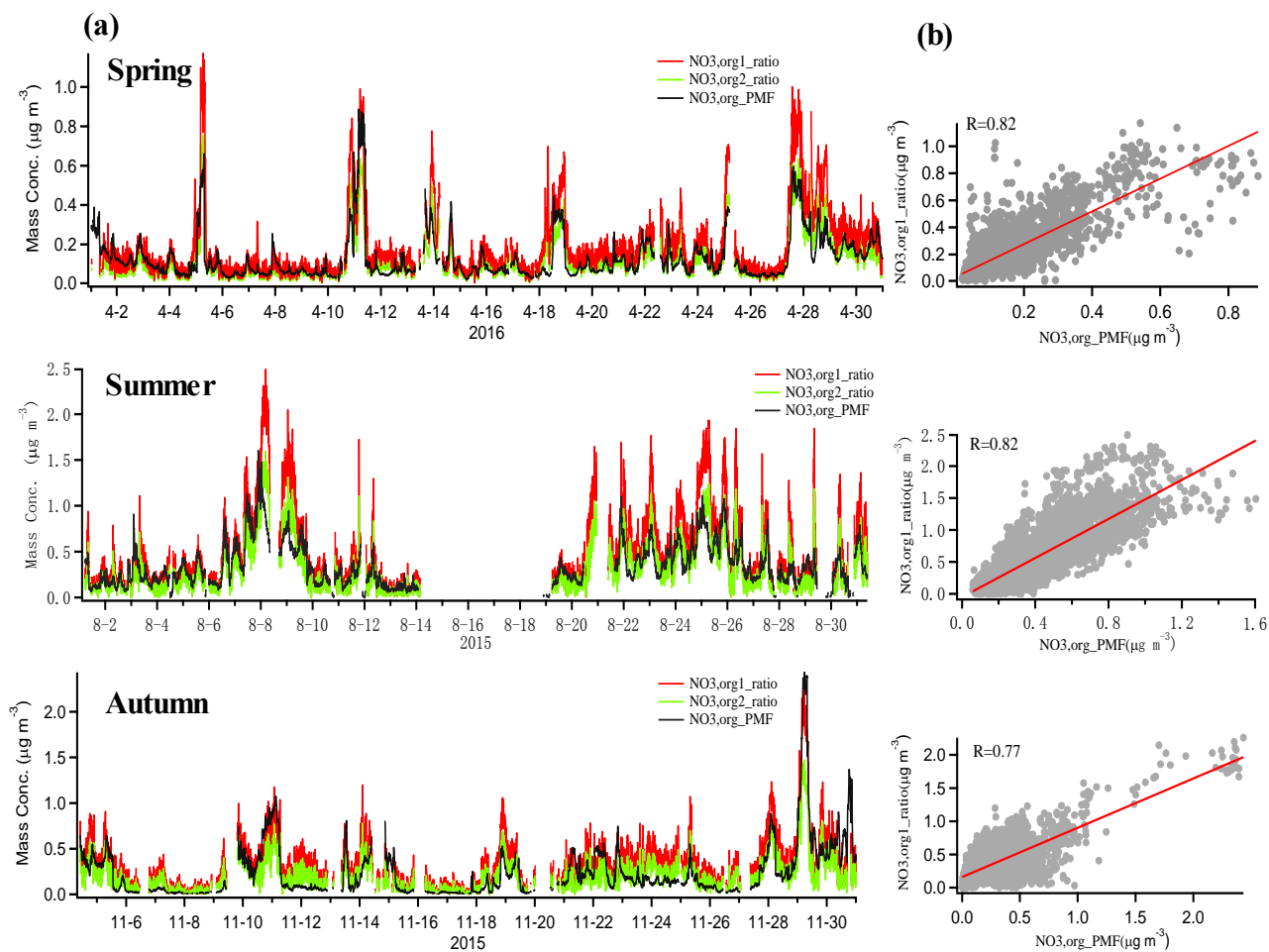
161 **Table 2.** A summary of organic nitrate estimations via the $\text{NO}^+/\text{NO}_2^+$ ratio method and PMF method

Sampling period	NO ⁺ /NO ₂ ⁺ ratio method				PMF method	
	NO _{3,org} (μg m ⁻³) ^a		NO _{3,org} /NO ₃		NO _{3,org} (μg m ⁻³) ^b	NO _{3,org} /NO ₃
	lower	upper	lower	upper		
Spring	0.12	0.19	13%	21%	0.12	12%
Summer	0.34	0.53	41%	64%	0.39	43%
Autumn	0.21	0.33	16%	25%	0.21	16%
Winter	/	/	/	/	/	/

162 ^a $\text{NO}_{3,\text{org}}$ for upper bounds is denoted as $\text{NO}_{3,\text{org1_ratio}}$, and $\text{NO}_{3,\text{org}}$ for lower bounds is denoted as $\text{NO}_{3,\text{org2_ratio}}$

163 ^b $\text{NO}_{3,\text{org}}$ estimated using the PMF method is denoted as $\text{NO}_{3,\text{org_PMF}}$

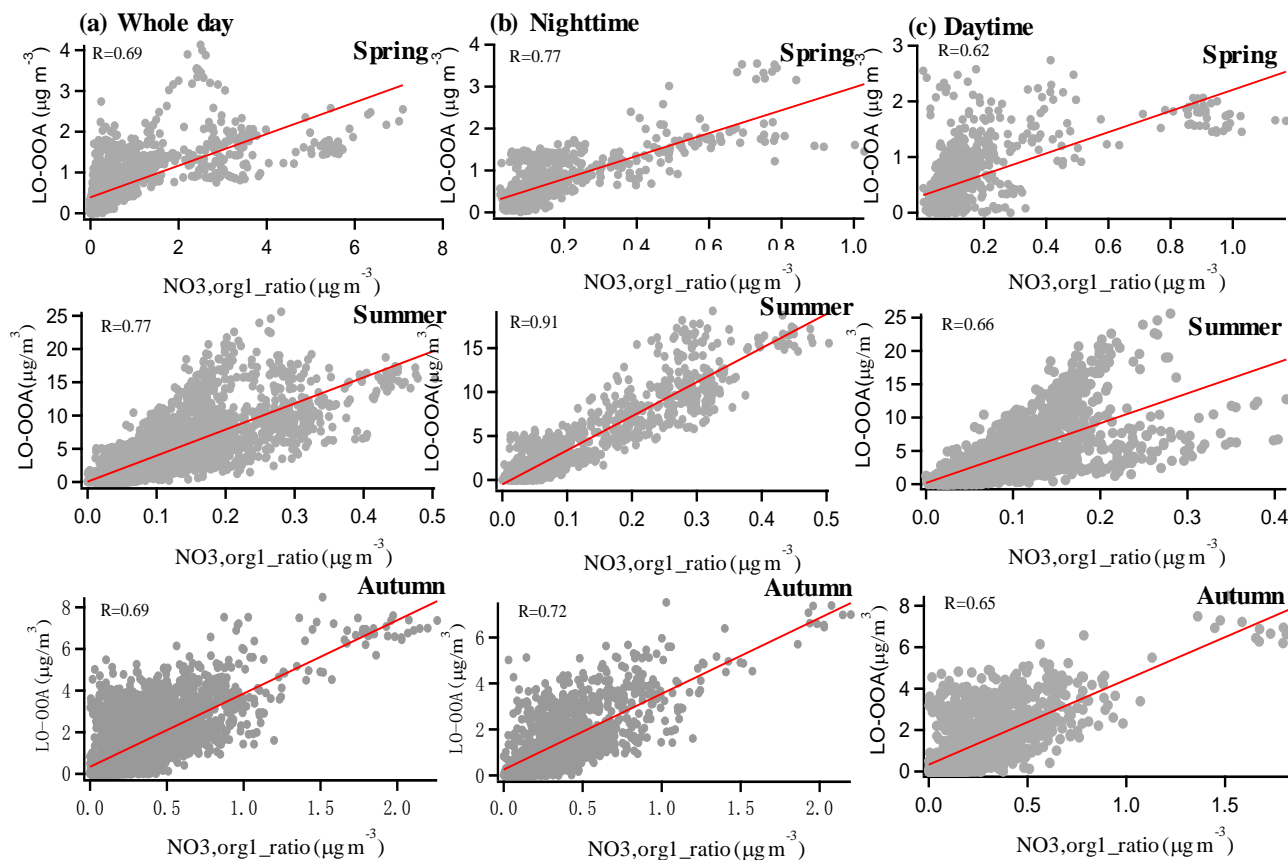
164 To verify the reliability of the estimated results, each $\text{NO}_{3,\text{org}}$ concentration time series calculated by these two methods is
 165 shown in Figure 2, and the correlation coefficient (R) for each season is adequate (0.82 for spring, 0.82 for summer and 0.77
 166 for autumn), indicating that similar results are achieved by using the $\text{NO}^+/\text{NO}_2^+$ ratio method and PMF method. To summarize,
 167 we chose a reliable estimation range of $\text{NO}_{3,\text{org}}$ for each season: 0.12 to 0.19 $\mu\text{g m}^{-3}$ for spring, 0.34 to 0.53 $\mu\text{g m}^{-3}$ for summer
 168 and 0.21 to 0.33 $\mu\text{g m}^{-3}$ for autumn. Furthermore, we found that organic nitrates contribute 9-21% to OAs in spring, 11-25%
 169 in summer and 9-20% in autumn based on the reliable estimation range of the $\text{NO}_{3,\text{org}}$ concentration and the assumption that
 170 the average molecular weight of organic nitrates ranges from 200 g mol^{-1} to 300 g mol^{-1} (Rollins et al., 2012). The level of
 171 $\text{NO}_{3,\text{org}}$ is highest during the summer in Shenzhen, which is consistent with the seasonal variations in literatures (Ng et al.,
 172 2017). In addition, it is seen that the difference in the $\text{NO}_{3,\text{org}}$ mass concentration between South China and the southeastem
 173 USA is small, even though the levels of anthropogenic emission species (such as BC and NO_x) are much higher in South China
 174 than those in southeastern USA (Xu et al., 2015b); this implies that aerosol ONs might not be closely related to anthropogenic
 175 emissions.



176

177 **Figure 2.** (a) Time series of $\text{NO}_{3,\text{org}}$ concentrations estimated by the $\text{NO}^+/\text{NO}_2^+$ ratio method and PMF method for each178 season, (b) scatterplots of $\text{NO}_{3,\text{org1_ratio}}$ and $\text{NO}_{3,\text{org_PMF}}$.179 **3.2 Correlation between organic nitrates and LO-OOA**

180 In this study, we also performed a PMF analysis on both organic spectra solely to investigate OA source apportionment. The
181 same organic factors were identified as those in the PMF analysis on organics, combined with NO_x^+ ions, including HOAs,
182 LO-OOAs and MO-OOAs. For the total daily data, organic nitrates were better-correlated with LO-OOAs than with any other
183 factor. Then, we further found a noticeably improved correlation between the LO-OOAs and organic nitrates at night (20:00-
184 6:00) and a decreased correlation during the daytime (7:00-19:00) in Figure 3. The biggest improvement is seen in summer,
185 where the correlation coefficient (R) increases from 0.77 for the whole day to 0.91 at night. Considering the relatively high
186 BVOC emissions during the summer in Shenzhen (Zhu et al., 2012), the summer LO-OOAs may be closely related to the
187 oxidation of BVOCs, especially at nighttime.



188

189

Figure 3. Scatter plots of $\text{NO}_{3,\text{org1_ratio}}$ and LO-OOA for each season for the whole day (a), at nighttime (b) and during the day (c).

190

191

3.3 Nighttime formation of organic nitrates in particles

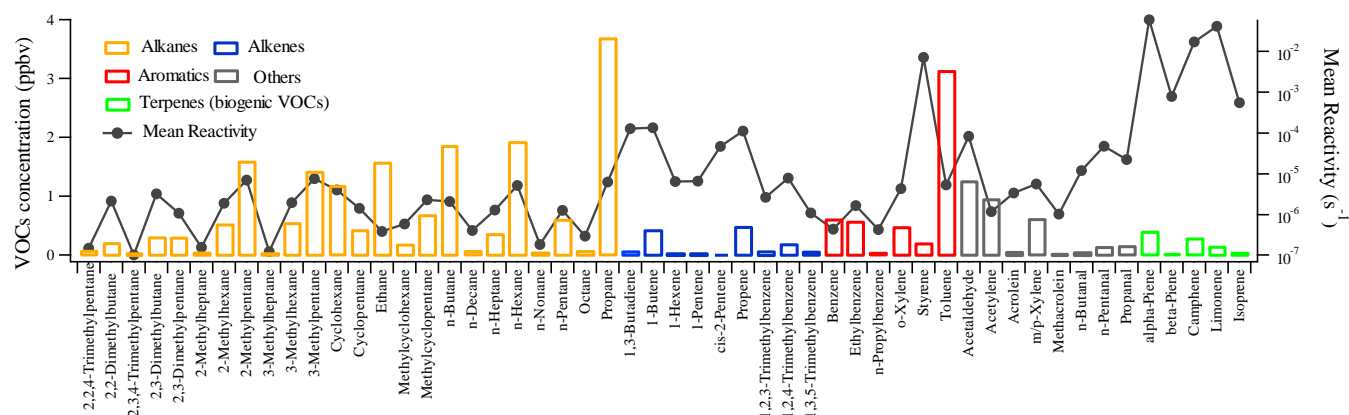
192

In this section, we will further investigate the potential formation pathway of organic nitrates at night according to the analysis of particulate organic nitrates in southeastern USA in Xu et al. (2015a). Since on-line VOCs measurement with an automated in situ gas-chromatography mass spectrometer (GC-MS) was only performed during the spring campaign, the following theoretical analysis is just applied to the dataset for the spring case. According to Figure 4, the concentrations of anthropogenic VOC species, such as propane and toluene, were dozens of times higher than those of biogenic VOCs at night. However, based on the estimation method in Section 2.3, two biogenic VOCs, i.e., limonene and α -pinene, were identified as the key VOC precursors, accounting for approximately 90% of the NO_3 lost due to the reactions with VOCs. Thus, the nighttime SOA production from limonene and α -pinene with NO_3 was further calculated (Text S1). The results showed that the estimated mass concentration range ($0.15\text{--}1.29 \mu\text{g m}^{-3}$) for SOAs agrees well with the range ($0.38\text{--}0.87 \mu\text{g m}^{-3}$) of organic nitrate concentrations at night. And noted that SOA yields from limonene + NO_3 is much higher than α -pinene + NO_3 (Hallquist et al., 1999; Fry et al., 2011, 2014; Spittler et al., 2006; Boyd et al., 2017). The diurnal patterns of the mass concentrations in the

202



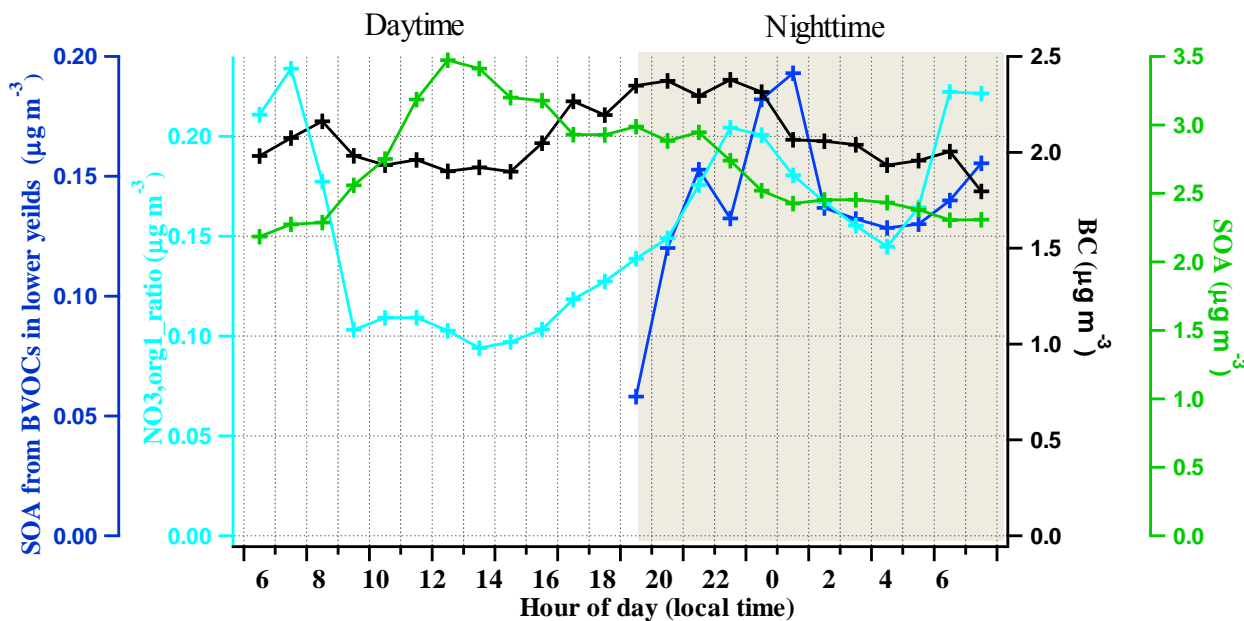
203 measured BC, SOA (LO-OOA+MO-OOA) resolved by PMF, organic nitrate functionality ($\text{NO}_{3,\text{org1_ratio}}$) and SOAs from the
204 BVOC+ NO_3 in the low SOA yield are shown in Figure 5. The concentration of BC is low during the daytime, with a planetary
205 boundary layer (PBL) height that is increased, while the concentration increases in the early evening due to the effects of both
206 the lower PBL and rush hour traffic (He et al., 2011). Compared to BC, the organic nitrate concentration shows a much more
207 distinct variation trend, with low mass loading in the daytime and high mass loading at night, and it has two unique rapid-
208 growth processes (19:00-22:00 and 3:00-6:00) after sunset, which cannot be explained by the PBL variation. Especially, the
209 second increase in organic nitrates from 3:00-6:00 clearly suggests significant nighttime SOA formation. Compared to the
210 bulk SOA, which shows an increase in the daytime related to photochemical formation while a steady level after midnight, the
211 concentration of organic nitrates increases from 3:00-6:00 also clearly indicates different formation mechanism. However, the
212 SOA of our theoretical calculation based on BVOCs and NO_3 indeed shows two similar increasing processes, well explaining
213 the observed trends. Since the similar nighttime formation trend for organic nitrates from biogenic emissions was also seen in
214 a forest environment in Finland (Yan et al., 2016), the results in this study shows that the BVOC+ NO_3 chemistry is also
215 potentially critical for the formation of nighttime organic nitrates even in a polluted urban atmosphere.
216



217

218

Figure 4. The mean concentrations of VOCs and the corresponding NO_3 reactivity at night during the spring campaign.



219

220

Figure 5. Diurnal trends of measured BC, SOA resolved by PMF, organic nitrate functionality ($\text{NO}_{3,\text{org1_ratio}}$), and SOA from BVOC+ NO_3 in a low SOA yield.

221

222

4. Conclusions

223

An Aerodyne HR-ToF-AMS was deployed in urban Shenzhen in South China for one month per season during 2015–2016 to characterize particulate organic nitrates with high time resolution. We find that the mass fraction of organic nitrates in the total measured nitrates is substantial during warm seasons, including spring (13–21%), summer (41–64%) and autumn (16–25%), while the contribution is negligible during winter in South China. The comparison analysis between organic nitrates and each OA factor for different periods of the day shows good correlations ($R=0.77$ in spring, 0.91 in summer and 0.72 in autumn) between organic nitrates and the LO-OOA factor at nighttime. Based on this, we further investigate the potential pathway for the formation of nighttime organic nitrates, and the results suggest that the BVOCs+ NO_3 chemistry plays a key role in the formation of nighttime organic nitrates and SOAs, and limonene is the most important precursors of VOCs for this type of reaction. Overall, we infer that, even in polluted urban atmosphere with high abundance of anthropogenic pollutants, particle-phase organic nitrates are possibly mostly derived from the formation from biogenic VOCs, and may be a good surrogate for studying the effects of biogenic emissions on air pollution and the climate.

233

234 **Acknowledgments**

235 This work was supported by the Ministry of Science and Technology of China (2018YFC0213901), the National Natural
236 Science Foundation of China (91544215; 41622304) and the Science and Technology Plan of Shenzhen Municipality.

237 **References**

- 238 Ayres, B.R., Allen, H.M., Draper, D.C., Brown, S.S., Wild, R.J., Jimenez, J.L., Day, D.A., Campuzano-Jost, P., Hu, W., De
239 Gouw, J.A., Koss, A., Cohen, R.C., Duffey, K.C., Romer, P., Baumann, K., Edgerton, E., Takahama, S., Thornton, J.A.,
240 Lee, B.H., Lopez-Hilfiker, F.D., Mohr, C., Wennberg, P.O., Nguyen, T.B., Teng, A.P., Goldstein, A.H., Olson, K., Fry,
241 J.L.: Organic nitrate aerosol formation via NO₃+ biogenic volatile organic compounds in the southeastern United States.
242 Atmos. Chem. Phys. 15, 13377-13392. <https://doi.org/10.5194/acp-15-13377-2015>, 2015.
- 243 Boyd, C.M., Nah, T., Xu, L., Berkemeier, T., Ng, N.L.: Secondary Organic Aerosol (SOA) from Nitrate Radical Oxidation
244 of Monoterpenes: Effects of Temperature, Dilution, and Humidity on Aerosol Formation, Mixing, and Evaporation.
245 Environ. Sci. Technol. 51, 7831–7841. <https://doi.org/10.1021/acs.est.7b01460>, 2017.
- 246 Boyd, C.M., Sanchez, J., Xu, L., Eugene, A.J., Nah, T., Tuet, W.Y., Guzman, M.I., Ng, N.L.: Secondary organic aerosol
247 formation from the β -pinene+NO₃ system: effect of humidity and peroxy radical fate. Atmos. Chem. Phys. 15, 7497-
248 7522. <https://doi.org/10.5194/acp-15-7497-2015>, 2015.
- 249 Bruns, E.A., Perraud, V., Zelenyuk, A., Ezell, M.J., Johnson, S.N., Yu, Y., Imre, D., Finlayson-Pitts, B.J., Alexander, M.L.:
250 Comparison of FTIR and particle mass spectrometry for the measurement of particulate organic nitrates. Environ. Sci.
251 Technol. 44, 1056-1061. <https://doi.org/10.1021/es9029864>, 2010.
- 252 Canagaratna, M.R., Jayne, J.T., Jimenez, J.L., Allan, J.D., Alfarra, M.R., Zhang, Q., Onasch, T.B., Drewnick, F., Coe, H.,
253 Middlebrook, A., Delia, A., Williams, L.R., Trimborn, A.M., Northway, M.J., DeCarlo, P.F., Kolb, C.E., Davidovits, P.,
254 Worsnop, D.R.: Chemical and microphysical characterization of ambient aerosols with the aerodyne aerosol mass
255 spectrometer. Mass Spectrom. Rev. 26, 185-222. <https://doi.org/10.1002/mas.20115>, 2007.
- 256 Crowley, J.N., Thieser, J., Tang, M.J., Schuster, G., Bozem, H., Beygi, Z.H., Fischer, H., Diesch, J.M., Drewnick, F., Borrmann,
257 S., Song, W., Yassaa, N., Williams, J., Pöhler, D., Platt, U., Lelieveld, J.: Variable lifetimes and loss mechanisms for
258 NO₃ and N₂O₅ during the DOMINO campaign: Contrasts between marine, urban and continental air. Atmos. Chem. Phys.
259 11, 10853-10870. <https://doi.org/10.5194/acp-11-10853-2011>, 2011.
- 260 DeCarlo, P.F., Kimmel, J.R., Trimborn, A., Northway, M.J., Jayne, J.T., Aiken, A.C., Gonin, M., Fuhrer, K., Horvath, T.,
261 Docherty, K.S., Worsnop, D.R., Jimenez, J.L.: Field-deployable, high-resolution, time-of-flight aerosol mass
262 spectrometer. Anal. Chem. 78, 8281-8289. <https://doi.org/10.1021/ac061249n>, 2006.
- 263 Farmer, D.K., Matsunaga, A., Docherty, K.S., Surratt, J.D., Seinfeld, J.H., Ziemann, P.J., Jimenez, J.L.: Response of an aerosol
264 mass spectrometer to organonitrates and organosulfates and implications for atmospheric chemistry. Proc. Natl. Acad.
265 Sci. 107, 6670-6675. <https://doi.org/10.1073/pnas.0912340107>, 2010.



- 266 Fry, J.L., Draper, D.C., Barsanti, K.C., Smith, J.N., Ortega, J., Winkler, P.M., Lawler, M.J., Brown, S.S., Edwards, P.M.,
267 Cohen, R.C.: Secondary Organic Aerosol Formation and Organic Nitrate Yield from NO₃ Oxidation of Biogenic
268 Hydrocarbons. *Environ. Sci. Technol.* 48, 11944–11953. <https://doi.org/10.1021/es502204x>, 2014.
- 269 Fry, J.L., Draper, D.C., Zarzana, K.J., Campuzano-Jost, P., Day, D.A., Jimenez, J.L., Brown, S.S., Cohen, R.C., Kaser, L.,
270 Hansel, A., Cappellin, L., Karl, T., Hodzic Roux, A., Turnipseed, A., Cantrell, C., Lefer, B.L., Grossberg, N.:
271 Observations of gas- and aerosol-phase organic nitrates at BEACHON-RoMBAS 2011. *Atmos. Chem. Phys.* 13, 8585-
272 8605. <https://doi.org/10.5194/acp-13-8585-2013>, 2013.
- 273 Fry, J.L., Kiendler-Scharr, A., Rollins, A.W., Brauers, T., Brown, S.S., Dorn, H.P., Dubé, W.P., Fuchs, H., Mensah, A.,
274 Rohrer, F., Tillmann, R., Wahner, A., Wooldridge, P.J., Cohen, R.C.: SOA from limonene: Role of NO₃ in its
275 generation and degradation. *Atmos. Chem. Phys.* 11, 3879-3894. <https://doi.org/10.5194/acp-11-3879-2011>, 2011.
- 276 Fry, J.L., Kiendler-Scharr, A., Rollins, A.W., Wooldridge, P.J., Brown, S.S., Fuchs, H., Dube, W.P., Mensah, A., Dal Maso,
277 M., Tillmann, R.: Organic nitrate and secondary organic aerosol yield from NO₃ oxidation of β-pinene evaluated using
278 a gas-phase kinetics/aerosol partitioning model. *Atmos. Chem. Phys.* 9, 1431–1449. [https://doi.org/10.5194/acp-9-1431-](https://doi.org/10.5194/acp-9-1431-2009)
279 [2009](https://doi.org/10.5194/acp-9-1431-2009), 2008.
- 280 Hallquist, M., Wängberg, I., Ljungström, E., Barnes, I., Becker, K.H.: Aerosol and product yields from NO₃radical-initiated
281 oxidation of selected monoterpenes. *Environ. Sci. Technol.* 33, 553-559. <https://doi.org/10.1021/es980292s>, 1999.
- 282 Hao, L.Q., Kortelainen, A., Romakkaniemi, S., Portin, H., Jaatinen, A., Leskinen, A., Komppula, M., Miettinen, P., Sueper,
283 D., Pajunoja, A., Smith, J.N., Lehtinen, K.E.J., Worsnop, D.R., Laaksonen, A., Virtanen, A.: Atmospheric submicron
284 aerosol composition and particulate organic nitrate formation in a boreal forestland-urban mixed region. *Atmos. Chem.*
285 *Phys.* 14, 13483-13495. <https://doi.org/10.5194/acp-14-13483-2014>, 2014.
- 286 He, L.Y., Huang, X.F., Xue, L., Hu, M., Lin, Y., Zheng, J., Zhang, R., Zhang, Y.H.: Submicron aerosol analysis and organic
287 source apportionment in an urban atmosphere in Pearl River Delta of China using high-resolution aerosol mass
288 spectrometry. *J. Geophys. Res. Atmos.* 116, D12. <https://doi.org/10.1029/2010JD014566>, 2011.
- 289 Huang, X.F., He, L.Y., Hu, M., Canagaratna, M.R., Sun, Y., Zhang, Q., Zhu, T., Xue, L., Zeng, L.W., Liu, X.G., Zhang, Y.H.,
290 Jayne, J.T., Ng, N.L., Worsnop, D.R.: Highly time-resolved chemical characterization of atmospheric submicron particles
291 during 2008 Beijing Olympic games using an aerodyne high-resolution aerosol mass spectrometer. *Atmos. Chem. Phys.*
292 10, 8933-8945. <https://doi.org/10.5194/acp-10-8933-2010>, 2010.
- 293 Huang, X.F., He, L.Y., Xue, L., Sun, T.L., Zeng, L.W., Gong, Z.H., Hu, M., Zhu, T.: Highly time-resolved chemical
294 characterization of atmospheric fine particles during 2010 Shanghai World Expo. *Atmos. Chem. Phys.* 12, 4897-4907.
295 <https://doi.org/10.5194/acp-12-4897-2012>, 2012.
- 296 Huang, X.F., Xue, L., Tian, X.D., Shao, W.W., Sun, T. Le, Gong, Z.H., Ju, W.W., Jiang, B., Hu, M., He, L.Y.: Highly time-
297 resolved carbonaceous aerosol characterization in Yangtze River Delta of China: Composition, mixing state and
298 secondary formation. *Atmos. Environ.* 64, 200-207. <https://doi.org/10.1016/j.atmosenv.2012.09.059>, 2013.



- 299 Lee, B.H., Mohr, C., Lopez-Hilfiker, F.D., Lutz, A., Hallquist, M., Lee, L., Romer, P., Cohen, R.C., Iyer, S., Kurten, T., Hu,
300 W., Day, D.A., Campuzano-Jost, P., Jimenez, J.L., Xu, L., Ng, N.L., Guo, H., Weber, R.J., Wild, R.J., Brown, S.S., Koss,
301 A., de Gouw, J., Olson, K., Goldstein, A.H., Seco, R., Kim, S., McAvey, K., Shepson, P.B., Starn, T., Baumann, K.,
302 Edgerton, E.S., Liu, J., Shilling, J.E., Miller, D.O., Brune, W., Schobesberger, S., D'Ambro, E.L., Thornton, J.A.: Highly
303 functionalized organic nitrates in the southeast United States: Contribution to secondary organic aerosol and reactive
304 nitrogen budgets. *Proc. Natl. Acad. Sci.* 113, 1516-1521. <https://doi.org/10.1073/pnas.1508108113>, 2016.
- 305 Lelieveld, J., Gromov, S., Pozzer, A., Taraborrelli, D.: Global tropospheric hydroxyl distribution, budget and reactivity. *Atmos.*
306 *Chem. Phys.* 16, 12477-12493. <https://doi.org/10.5194/acp-16-12477-2016>, 2016.
- 307 Middlebrook, A.M., Bahreini, R., Jimenez, J.L., Canagaratna, M.R.: Evaluation of composition-dependent collection
308 efficiencies for the Aerodyne aerosol mass spectrometer using field data. *Aerosol Sci. Technol.* 46, 258-271.
309 <https://doi.org/10.1080/02786826.2011.620041>, 2012.
- 310 Ng, N. L., Brown, S. S., Archibald, A. T., Atlas, E., Cohen, R. C., Crowley, J. N., Day, D. A., Donahue, N. M., Fry, J. L.,
311 Fuchs, H., Griffin, R. J., Guzman, M. I., Herrmann, H., Hodzic, A., Iinuma, Y., Jimenez, J. L., Kiendler-Scharr, A., Lee,
312 B. H., Luecken, D. J., Mao, J., McLaren, R., Mutzel, A., Osthoff, H. D., Ouyang, B., Picquet-Varrault, B., Platt, U., Pye,
313 H. O. T., Rudich, Y., Schwantes, R. H., Shiraiwa, M., Stutz, J., Thornton, J. A., Tilgner, A., Williams, B. J., and Zaveri,
314 R. A.: Nitrate radicals and biogenic volatile organic compounds: oxidation, mechanisms, and organic aerosol, *Atmos.*
315 *Chem. Phys.*, 17, 2103-2162, <https://doi.org/10.5194/acp-17-2103-2017>, 2017.
- 316 Ng, N. L., Canagaratna, M. R., Zhang, Q., Jimenez, J. L., Tian, J., Ulbrich, I. M., Kroll, J. H., Docherty, K.S., Chhabra, P.S.,
317 Bahreini, R., Murphy, S.M., Seinfeld, J.H., Hildebrandt, L., Donahue, N.M., Decarlo, P.F., Lanz, V.A., Prévôt, A.S.H.,
318 Dinar, E., Rudich, Y., Worsnop, D.R.: Organic aerosol components observed in Northern Hemispheric datasets from
319 Aerosol Mass Spectrometry. *Atmos. Chem. Phys.* 10, 4625-4641. <https://doi.org/10.5194/acp-10-4625-2010>, 2010.
- 320 Rollins, A.W., Browne, E.C., Min, K.-E., Pusede, S.E., Wooldridge, P.J., Gentner, D.R., Goldstein, A.H., Liu, S., Day, D.A.,
321 Russell, L.M., Cohen, R.C.: Evidence for NO_x Control over Nighttime SOA Formation. *Science*. 337, 1210-1212.
322 <https://doi.org/10.1126/science.1221520>, 2012.
- 323 Sato, K., Takami, A., Iozaki, T., Hikida, T., Shimono, A., Imamura, T.: Mass spectrometric study of secondary organic aerosol
324 formed from the photo-oxidation of aromatic hydrocarbons. *Atmos. Environ.* 44, 1080-1087.
325 <https://doi.org/10.1016/j.atmosenv.2009.12.013>, 2010.
- 326 Saunders, S.M., Jenkin, M.E., Derwent, R.G., Pilling, M.J.: Protocol for the development of the Master Chemical Mechanism,
327 MCM v3 (Part A): tropospheric degradation of non-aromatic volatile organic compounds. *Atmos. Chem. Phys.* 3, 161-
328 180. <https://doi.org/10.5194/acp-3-161-2003>, 2002.
- 329 Sobanski, N., Thieser, J., Schuladen, J., Sauvage, C., Song, W., Williams, J., Lelieveld, J., Crowley, J.N.: Day and night-time
330 formation of organic nitrates at a forested mountain site in south-west Germany. *Atmos. Chem. Phys.* 17, 4115-
331 4130. <https://doi.org/10.5194/acp-17-4115-2017>, 2017.



- 332 Spittler, M., Barnes, I., Bejan, I., Brockmann, K.J., Benter, T., Wirtz, K.: Reactions of NO₃ radicals with limonene and α -
333 pinene : Product and SOA formation. *Atmos. Environ.* 40, 116–127. <https://doi.org/10.1016/j.atmosenv.2005.09.093>,
334 2006.
- 335 Sun, Y., Zhang, Q., Schwab, J.J., Yang, T., Ng, N.L., Demerjian, K.L.: Factor analysis of combined organic and inorganic
336 aerosol mass spectra from high resolution aerosol mass spectrometer measurements. *Atmos. Chem. Phys.* 12, 8537–8551.
337 <https://doi.org/10.5194/acp-12-8537-2012>, 2012.
- 338 Teng, A.P., Crounse, J.D., Lee, L., St. Clair, J.M., Cohen, R.C., Wennberg, P.O.: Hydroxy nitrate production in the OH-
339 initiated oxidation of alkenes. *Atmos. Chem. Phys.* 13, 5367–5377. <https://doi.org/10.5194/acp-13-5367-2015>, 2015.
- 340 Teng, A.P., Crounse, J.D., Wennberg, P.O.: Isoprene Peroxy Radical Dynamics. *J. Am. Chem. Soc.* 139, 4297–4316.
341 <https://doi.org/10.1021/jacs.6b12838>, 2017.
- 342 Xu, L., Guo, H., Boyd, C.M., Klein, M., Bougiatioti, A., Cerully, K.M., Hite, J.R., Isaacman-VanWertz, G., Kreisberg, N.M.,
343 Knote, C., Olson, K., Koss, A., Goldstein, A.H., Hering, S. V., de Gouw, J., Baumann, K., Lee, S.-H., Nenes, A., Weber,
344 R.J., Ng, N.L.: Effects of anthropogenic emissions on aerosol formation from isoprene and monoterpenes in the
345 southeastern United States. *Proc. Natl. Acad. Sci.* 112, 37–42. <https://doi.org/10.1073/pnas.1417609112>, 2015a.
- 346 Xu, L., Suresh, S., Guo, H., Weber, R.J., Ng, N.L.: Aerosol characterization over the southeastern United States using high-
347 resolution aerosol mass spectrometry: Spatial and seasonal variation of aerosol composition and sources with a focus on
348 organic nitrates. *Atmos. Chem. Phys.* 15, 7307–7336. <https://doi.org/10.5194/acp-15-7307-2015>, 2015b.
- 349 Xu, W., Sun, Y., Wang, Q., Du, W., Zhao, J., Ge, X., Han, T., Zhang, Y., Zhou, W., Li, J., Fu, P., Wang, Z., Worsnop, D.R.:
350 Seasonal Characterization of Organic Nitrogen in Atmospheric Aerosols Using High Resolution Aerosol Mass
351 Spectrometry in Beijing, China. *ACS Earth Sp. Chem.* 1, 673–682. <https://doi.org/10.1021/acsearthspacechem.7b00106>,
352 2017.
- 353 Yan, C., Nie, W., Äijälä, M., Rissanen, M.P., Canagaratna, M.R., Massoli, P., Junninen, H., Jokinen, T., Sarnela, N., Häme,
354 S.A.K., Schobesberger, S., Canonaco, F., Yao, L., Prévôt, A.S.H., Petäjä, T., Kulmala, M., Sipilä, M., Worsnop, D.R.,
355 Ehn, M.: Source characterization of highly oxidized multifunctional compounds in a boreal forest environment using
356 positive matrix factorization. *Atmos. Chem. Phys.* 16, 12715–12731. <https://doi.org/10.5194/acp-16-12715-2016>, 2016.
- 357 Zhang, Q., Jimenez, J.L., Canagaratna, M.R., Ulbrich, I.M., Ng, N.L., Worsnop, D.R., Sun, Y.: Understanding atmospheric
358 organic aerosols via factor analysis of aerosol mass spectrometry: A review. *Anal. Bioanal. Chem.* 401, 3045–3067.
359 <https://doi.org/10.1007/s00216-011-5355-y>, 2011.
- 360 Zhang, Y.H., Su, H., Zhong, L.J., Cheng, Y.F., Zeng, L.M., Wang, X.S., Xiang, Y.R., Wang, J.L., Gao, D.F., Shao, M., Fan,
361 S.J., Liu, S.C.: Regional ozone pollution and observation-based approach for analyzing ozone-precursor relationship
362 during the PRIDE-PRD2004 campaign. *Atmos. Environ.* 42, 6203–6218. <https://doi.org/10.1016/j.atmosenv.2008.05.002>,
363 2008.



- 364 Zhu, Q., He, L.Y., Huang, X.F., Cao, L.M., Gong, Z.H., Wang, C., Zhuang, X., Hu, M.: Atmospheric aerosol compositions
365 and sources at two national background sites in northern and southern China. Atmos. Chem. Phys. 16, 10283-10297.
366 <https://doi.org/10.5194/acp-16-10283-2016>, 2016.
- 367 Zhu, S. F.; Huang, X. F.; Ling-Yan, H. E.; Si-Hua, L. U.; Feng, N.: Variation characteristics and chemical reactivity of ambient
368 VOCs in Shenzhen. China Environmental Science. 32, 2140-2148, 2012.
- 369